

Elsevier required licence: © <2020>. This manuscript version is made available under the CC-BY-NC-ND 4.0 license <http://creativecommons.org/licenses/by-nc-nd/4.0/>. The definitive publisher version is available online at [insert DOI]

1 **Hollow fiber membranes with hierarchical spherulite structure by thermally induced**
2 **phase separation using triple-orifice spinneret for membrane distillation**

3

4 Chuanjie Fang ^a, Wenyi Liu ^a, Pengfei Zhang ^a, Saeid Rajabzadeh ^a, Noriaki Kato ^a, Yuji
5 Sasaki ^a, Ho Kyong Shon ^b, Hideto Matsuyama ^{a*}

6

7 ^a *Research Center for Membrane and Film Technology, Department of Chemical Science and*
8 *Engineering, Kobe University, Rokkodaicho 1-1, Nada, Kobe 657-8501, Japan*

9

10 ^b *Centre for Technology in Water and Wastewater (CTWW), School of Civil and*
11 *Environmental Engineering, University of Technology, Sydney (UTS), P.O. Box 123,*
12 *Broadway, NSW 2007, Australia*

13

14 ** Corresponding author: Professor H. Matsuyama*

15 *E-mail address: matuyama@kobe-u.ac.jp (H. Matsuyama)*

16 *Tel. / Fax: +81 78 803 6180*

17

18

19

20

21

22

1 **Abstract**

2 In this study, polyvinylidene fluoride (PVDF) hollow fiber membranes were
3 developed by the thermally induced phase separation (TIPS) process using a triple-orifice
4 spinneret with solvent co-extrusion at the outermost channel for the application to membrane
5 distillation (MD). The polymer surface concentration during the membrane preparation was
6 controlled triggering the interfacial behaviors of diluent and polymer towards the extruded
7 solvent surface. The membrane surface was therefore controlled from dense to porous
8 structure with large pore size and high porosity, which considerably enhanced membrane
9 water vapor permeability to $13.5 \text{ L m}^{-2} \text{ h}^{-1}$. Furthermore, the solvent co-extrusion was
10 responsible for the formation of surface spherulites with different shapes, such as contacted
11 spherulites, isolated spherulite, and isolated spherulite with humps. The spherulites with
12 humps constructed a novel hierarchical structure, which brought about a superhydrophobic
13 surface that conferred the PVDF membrane remarkable wetting resistance in the MD process
14 towards the low-surface-tension saline water. More significantly, all the unique structures
15 were achieved using the one-step membrane fabrication process of solvent co-extrusion
16 without additional processes and materials. Thus, this work can provide a new, simple, and
17 useful alternative to achieve the preparation of the hollow fiber membranes with high MD
18 performances.

19

20 **Keywords:** Membrane distillation; Desalination; Thermally induced phase separation;
21 Hollow fiber membrane; Triple-orifice spinneret

22

1 **1. Introduction**

2 Desalination of seawater and brackish groundwater is a promising alternative to
3 obtain freshwater, which favorably alleviates the current and future water supply scarcity [1].
4 Membrane-based technology shows great potential to achieve this goal, such as reverse
5 osmosis, membrane distillation (MD), and electrodialysis. Among them, MD has attracted
6 broad attention due to its unique advantages, e.g., low energy consumption with high-
7 efficiency utilization in low-grade waste heat or other renewable energy resources [2], low
8 operating pressure [3], ultra-high salt rejection near 100%, and low sensitivity to salt
9 concentration [4]. Desalination by MD is a thermally driven separation process, which is
10 achieved using a hydrophobic microporous membrane that favors the water vapor permeation
11 based on pressure gradient, but impedes the saline water flow through the membrane due to
12 the membrane hydrophobic property. Like other membrane processes, membrane plays a
13 significant role in this technology to achieve high-efficiency desalination.

14 Membranes used in MD are mainly hydrophobic microfiltration membranes such as
15 polypropylene, polyethylene, polytetrafluoroethylene, and polyvinylidene fluoride (PVDF)
16 membranes with different shapes including hollow fiber, flat sheet, and tube prepared using
17 non-solvent induced phase separation (NIPS), thermally induced phase separation (TIPS),
18 electrospinning, or double stretching [5]. Although these prepared membranes have pore
19 structures suitable for high water vapor permeation, they fail to resist wetting from saline
20 water, especially, against seawater with complicated low surface tension components, due to
21 inadequate hydrophobicity [3, 6, 7]. Hence, recent advances in MD membranes have focused
22 on the modification of membrane surface structure to enhance hydrophobicity or

1 omniphobicity constructing micro-nano or re-entrant structures using nanoparticles or
2 nanoarrays [3, 6-9], or on the decrease of surface free energy to enhance hydrophobicity by
3 loading perfluorinated materials [6, 10-12]. Although these methods can significantly
4 increase the membrane wetting resistance, they include the complicated process which sets
5 up the obstacle for the actual applications. This indicates that a simple and feasible method
6 is highly required to simultaneously tailor the membrane pore structure and surface
7 hydrophobicity for high permeability and wetting resistance of the MD membranes.

8 Solvent co-extrusion at the outermost layer of a triple-orifice spinneret has recently
9 been developed to prepare hollow fiber and flat membrane in the TIPS process [13-18]. In
10 this method, in addition to controlling the membrane surface pore structure for enhancing
11 water permeability, it was observed that the structure near the surface showed an interesting
12 morphology with lots of micro-spherulites in the interconnected structures when using PVDF
13 as the membrane material [14]. This composite-like structure was fully different from the
14 normal porous morphology prepared in the NIPS process using the tripe-orifice spinneret
15 [19]. This special structure was due to the solid-liquid (S-L) phase separation in the TIPS
16 process induced by the solvent penetration into the polymer solution [16]. Furthermore, the
17 growth of the spherulite structure at the surface and sub-layer of the PVDF hollow fiber
18 membrane was controlled by co-extruding nucleation agent solution, and the tailored
19 spherulite surface structure showed a promising potential of enhancing the membrane surface
20 hydrophobicity [20].

21 The aim of this work is to develop the PVDF hollow fiber membrane with a novel
22 hierarchical spherulite structure having ultra-high hydrophobicity for the MD process by this

1 method of solvent co-extrusion using a triple-orifice spinneret in the TIPS process. Herein,
2 propylene carbonate (PC) was used as a diluent to prepare PVDF solution and an S-L phase
3 separation occurred upon cooling. A series of solvents having different compatibilities with
4 PC and PVDF were used to investigate the tailoring of the membrane surface pore structure
5 from dense to porous and the hierarchical spherulite structure of isolated micro-spherulite
6 with nano-humps. The controlled surface pore structure and hierarchical spherulite structure
7 were thoroughly characterized to analyze their effects on the membrane pore size, porosity,
8 and hydrophobicity. Furthermore, the membrane desalination and wetting resistance
9 performances were evaluated using a direct contact membrane distillation. To the best of our
10 knowledge, this is the first demonstration to achieve the preparation of PVDF hollow fiber
11 membranes with the hierarchical spherulite surface structure for high efficient MD
12 desalination.

13

14 **2. Experimental**

15 **2.1. Materials**

16 PVDF (Solf 6020, Mw: 670–700 kDa) was friendly supplied by Solvay Soiexis K.K.
17 (Tokyo, Japan). Acetyl tributyl citrate (ATBC), glycerol triacetate (GTA), diethyl phthalate
18 (DEP), propylene carbonate (PC), sulfolane, gamma-butyrolactone (GBL), glycerol
19 carbonate (GC), sodium chloride (NaCl), sodium dodecyl sulfate (SDS), isopropanol, and
20 ethanol were purchased from Wako Pure Chemical Industries, Ltd. (Osaka, Japan).
21 Properties of the materials used for the membrane preparation are shown in Table 1. Porous
22 Material Inc. (PMI, Ithaca, USA) provided galwick for pore size measurement. Pure water

1 was obtained from a Millipore Milli-Q unit. All chemicals were used here as received without
 2 further purification.

3

4 **Table 1.** Properties of the materials used for membrane preparation.

	$^*\delta_d$ (MPa ^{0.5}) ^[21]	$^*\delta_p$ (MPa ^{0.5}) ^[21]	$^*\delta_h$ (MPa ^{0.5}) ^[21]	$^*\delta_t$ (MPa ^{0.5}) ^[21]	$ \delta(\text{Solvent})-\delta(\text{PVDF}) $	Viscosity (cP) ^[22]	Boiling/melting point (°C) ^[22]
PVDF	17.2	12.5	9.2	23.2	-	-	173 (melting point)
PC	17	7.4	10.8	21.46	1.74	2.5	242
ATBC	16.02	2.56	8.55	18.3	4.9	34	343
GTA	16.5	4.5	9.1	19.4	3.8	21-30	258
DEP	17.6	9.6	4.5	20.6	2.6	16.3	302
Sulfolane	18.4	16.6	7.4	25.86	2.66	10.34	285
GBL	19	16.6	7.4	26.3	3.1	1.7	204
GC	17	9.6	18.9	27.74	4.54	61.6	350

5 $^*\delta_d$, dispersion solubility parameter; δ_p , polar solubility parameter; δ_h , hydrogen bonding solubility parameter;
 6 and δ_t , total solubility parameter.

7

8 **2.2. Hollow fiber membrane preparation**

9 In this work, a twin-screw extruder was used for dissolving PVDF to be a
 10 homogeneous solution with an aid of a diluent (PC) at the temperature of 190 °C for
 11 hollow fiber membrane preparation. The apparatus is shown in Fig. S1. The obtained
 12 homogeneous PVDF solution was forced by a gear pump to flow through the middle
 13 channel of a triple-orifice spinneret (Fig. S1) for the hollow fiber formation. PC was
 14 used as bore liquid and extruded through the inner channel of the spinneret to form the
 15 lumen of the hollow fiber. On the other hand, several types of solvents (ATBC, GTA,
 16 DEP, PC, sulfolane, GBL, and GC) were extruded from the outermost channel of the
 17 spinneret to tailor the membrane surface spherulite structure. The detailed preparation
 18 procedure of the PVDF hollow fiber membrane is shown in supporting information

1 and the membrane preparation condition is shown in Table S1. In addition, a normal
2 PVDF hollow fiber membrane was prepared with the same conditions while without
3 extruding solvent for the comparison. The diameters and thicknesses of the prepared
4 PVDF membranes are shown in Table S2.

5

6 **2.3. Membrane characterization**

7 Membrane morphology was observed using a JEOL JSF-7500F field-emission
8 scanning electronic microscope (FE-SEM). Membrane surface roughness was
9 measured using a laser scanning microscopy (VK-8510, Keyence, Osaka, Japan).
10 Membrane surface pore size and porosity were analyzed based on the FE-SEM image
11 with the aid of ImageJ software (NIH), as introduced in references [10]. Membrane
12 mean pore size was measured using an LLP-1100A liquid-liquid porometer (PMI,
13 USA). Membrane bulk porosity was measured using a wet and dry method [13] and
14 the procedure is described in supporting information. Membrane hydrophobicity was
15 evaluated by water contact angle (WCA) measured using a Drop Master 300 contact
16 angle goniometer (Kyowa Interface Science Co., Japan). The WCA hysteresis was
17 also evaluated by changing the contact between water drop and membrane surface.
18 Membrane mechanical strength was measured using a precision tensile testing device
19 (Shimadzu AGS-J, Japan). The phase diagram of the PVDF/PC system was measured
20 by cooling at 10 °C/min using a hot stage (Linkam, Surrey, UK) with a microscope
21 (Olympus, Tokyo, Japan) and a differential scanning calorimeter (PerkinElmer DSC
22 8500, USA) [23].

1

2 **2.4. MD performances for desalination**

3 MD performances for desalination were measured by a direct contact membrane
4 distillation (DCMD) mode using a self-made laboratory-scale apparatus, as shown in Fig. 1.
5 The dried PVDF hollow membranes were sealed in a pipe using glue to make a module with
6 an effective area of 60 cm². In this work, a model seawater of 35 g L⁻¹ NaCl aqueous solution
7 was used as a feed solution and circulated at the shell side of the module with a rate of 400
8 mL min⁻¹ using a centrifugal pump. The feed solution temperature was normally controlled
9 at 60 °C by a heater to produce water vapor. In the tube side of the module, pure water with
10 a temperature of 20 °C controlled using a chiller was used as a condensate solution and
11 circulated with a rate of 200 mL min⁻¹ using a centrifugal pump. The initial volumes of the
12 feed and condensate solution (pure water) were 1 L and 0.5 L, respectively. Due to the vapor
13 pressure difference, the produced water vapor can permeate through the membrane and be
14 then collected at the tube side by condensation to be liquid using the condensate solution.
15 Water vapor permeability, L m⁻² h⁻¹, can be obtained by Eq. (1) as follows:

$$16 \quad J = \frac{m}{A\rho t} \quad (1)$$

17 where J is the membrane water vapor permeability (L m⁻² h⁻¹), m is the permeated water mass
18 (g), ρ is the water density (0.998 kg·L⁻¹, 20 °C), A is the membrane effective permeation area
19 (m²), and t is the permeation time (h). Each reported water vapor permeability was an average
20 value collected after 6 h measurement.

21 To evaluate the membrane salt rejection, an electrical conductivity meter (Horiba B-
22 771, Kyoto, Japan) was used to monitor the electrical conductivity of the solution in the

1 permeate side bath, as shown in Fig. 1. Although the conductivity of the permeated water
2 was not measured directly, it was calculated using the volumes of the permeated water and
3 the permeation side bath solution and the measured solution conductivity at the permeation
4 side bath. Salt rejection, R_{salt} (%), was calculated using Eq. (2) as follows:

$$5 \quad R_{\text{salt}} = \frac{C_{\text{F,Salt}} - C_{\text{P,Salt}}}{C_{\text{F,Salt}}} \times 100\% \quad (2)$$

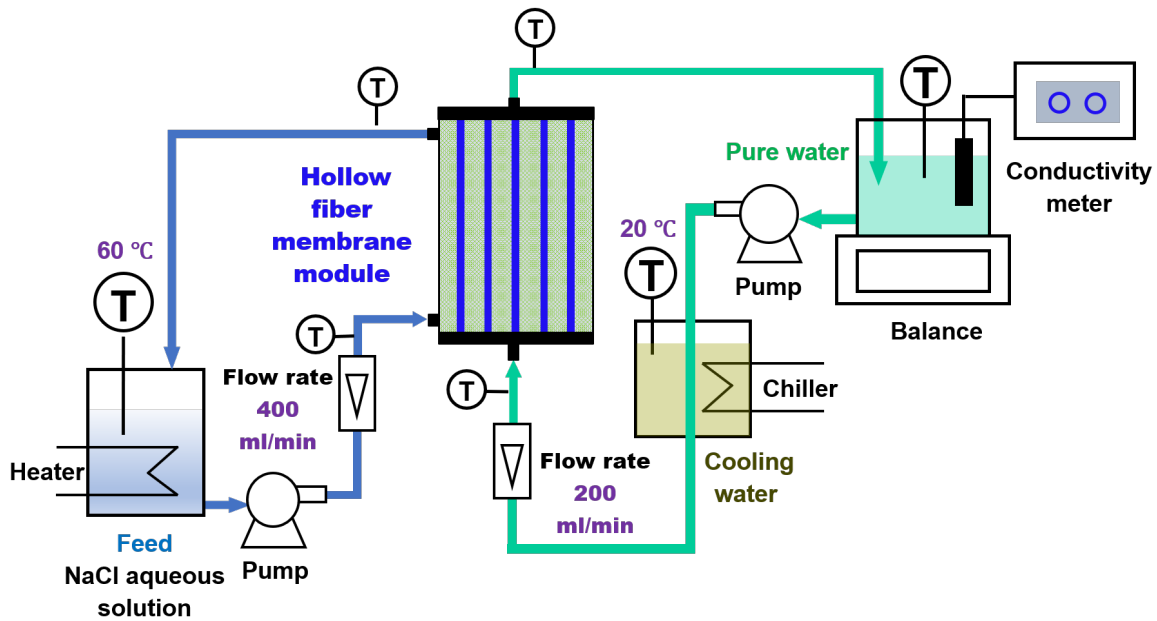
6 where, $C_{\text{F, Salt}}$, and $C_{\text{P, Salt}}$ are NaCl concentrations in the feed and permeated solutions, (g L^{-1}),
7 respectively.

8 Furthermore, the effects of salt concentration and temperature of the feed solution on
9 the MD performance were investigated by the same method as above using the PVDF
10 membrane prepared by extruding ATBC. Here, three salt concentrations (35, 70, and 105 g L^{-1})
11 and three temperatures (60, 70, and 80 °C) were used, respectively.

12 Membrane wetting resistance was evaluated using a low-surface-tension feed
13 solution. The low-surface-tension feed solution was prepared by adding a surfactant (SDS)
14 into 35 g L^{-1} NaCl aqueous solution of 60 °C. This is because the addition of SDS can
15 effectively decrease the surface tension of the feed solution, which increases the wetting
16 ability to membrane [24]. The SDS concentration in the feed solution was gradually increased
17 from 0.1 mM based on the membrane wetting resistance. To keep stable SDS concentration
18 in the feed solution (initial volume: 1 L) with fluctuation of less than 5 % after water vapor
19 permeation, pure water was added in feed solution when the volume loss reached to 50 mL.
20 The permeated water vapor was collected by pure water at 20 °C by condensation as
21 mentioned above. Here, the normalized membrane water vapor permeability (J/J_0) and real-

1 time salt rejection were used to evaluate the membrane wetting resistance. J and J_o are the
2 monitoring and initial water vapor permeability, respectively.

3 The long-term stability of the PVDF membrane was investigated using the membrane
4 prepared by extruding ATBC by increasing the operation period in the feed solution without
5 SDS.



7 **Fig. 1.** Schematic of a direct contact membrane distillation unit used in this study

8

9 **3. Results and discussion**

10 **3.1. Effect of co-extruded solvents on membrane morphology**

11 Figure 2 shows the membrane surface morphology using SEM images of PVDF
12 membrane prepared with and without co-extruded solvents. The respective membrane cross-
13 section morphologies are shown in Figs. S2 and S3. It was observed in Fig. 2(h) that the
14 normal PVDF membrane prepared without co-extruding solvent showed only a dense surface,

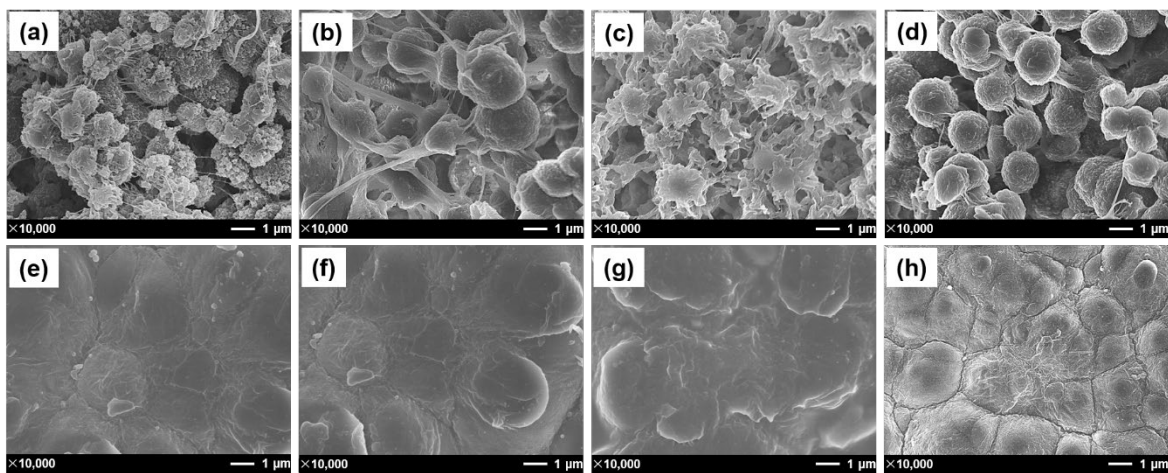
1 although the membrane bulk was the spherulitic structure (Figs. S2(h) and S3(h)). As shown
2 in Fig. S4, the phase separation mechanism in PVDF/PC system was a typical S-L phase
3 separation due to strong interaction between PC and PVDF, so that the spherulitic structure
4 formed at the membrane bulk. However, high diluent evaporation at the membrane surface
5 during the air gap increased PVDF surface concentration in the TIPS process [25, 26], which
6 strongly impeded the isolated spherulite formation. The formed spherulites were interacted
7 each other at the membrane surface. By contrast, when the solvents (ATBC, GTA, DEP, and
8 PC) were extruded in the membrane preparation, the prepared membranes had lots of
9 spherulites with a diameter in microscale (1-4 μm) at the membrane surface, and the
10 spherulites were isolated, as shown in Figs. 2(a, b, c, and d). On the other hand, when using
11 sulfolane, GBL, and GC as the extruded solvent, the membrane surface structures were dense
12 and are similar to that of the normal PVDF membrane, as shown in Figs. 2(e, f, and g). Hence,
13 it can be concluded that the membrane surface morphology was successfully controlled by
14 extruding different solvents. On the other hand, the membrane bulk structure remained
15 unchanged when changing the extruded solvent types (Figs. S2 and S3) because it was only
16 controlled by diluent (PC). Thus, the mechanical strengths of the prepared membranes were
17 hardly changed extruding the solvents (Fig. S5).

18 Previous studies reported that in the method of extruding the solvent, the movements
19 of diluent and polymer molecular chains from the bulk of dope solution towards the surface
20 contacting to the solvent occurred [13, 14, 23]. This changed the polymer surface
21 concentration and then controlled the membrane surface structure. When the extruded
22 solvents have better interaction with diluent than polymer, the diluent movement towards the

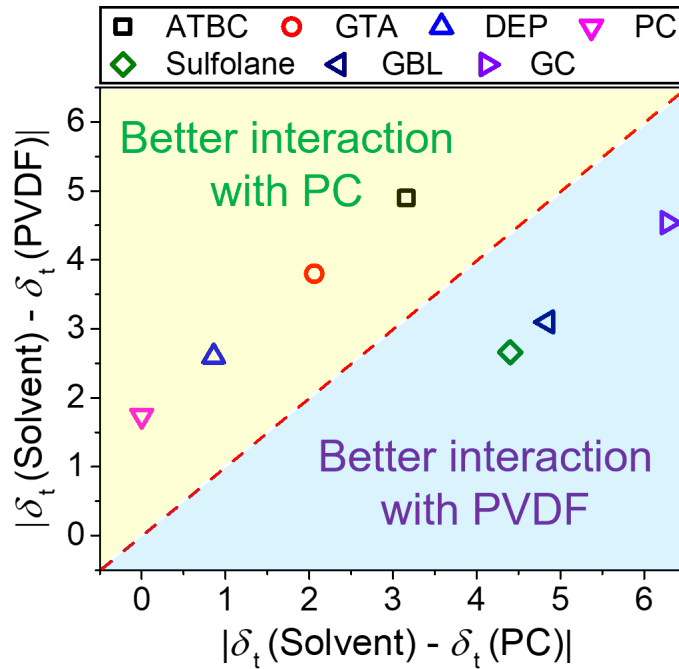
1 surface favorably happens and decreases the polymer surface concentration, which gives the
2 membrane a porous structure [23]. On the other hand, if the solvents have better interaction
3 with polymer than diluent, the polymer molecular chains are likely to move towards the
4 surface to increase the polymer surface concentration, so that the membrane surface becomes
5 dense [23]. In this work, the ternary interactions among solvent, diluent (PC), and polymer
6 (PVDF) were evaluated using the solubility parameter theory shown in Fig. 3 [13, 14]. The
7 x-axis is the difference of the total solubility parameter between solvent and diluent
8 ($|\delta(\text{Solvent})-\delta(\text{PC})|$). The lower this value, the better interaction between solvent and PC
9 (diluent). On the other hand, the y-axis ($|\delta(\text{Solvent})-\delta(\text{PVDF})|$) shows the interaction
10 between solvent and polymer. It was observed that ATBC, GTA, DEP, and PC were above
11 the diagonal line, showing better interaction of the extruded solvents with PC than PVDF.
12 Therefore, PC moves towards the surface, and favorably decreases the polymer surface
13 concentration. As a result, the formed spherulite was isolated to provide a porous surface due
14 to the existence of a large amount of diluent, as shown in Fig. 2(a, b, c, and d). By contrast,
15 sulfolane, GBL, and GC have better interaction with PVDF than PC, which induces the
16 movement of PVDF molecular chains towards the surface, and the PVDF surface
17 concentration increases. Accordingly, the prepared membranes showed a dense and
18 spherulite-contacted surface (Fig. 2(e, f, and g)). Thus, the ternary interaction among solvent,
19 diluent, and polymer plays a significant role in controlling the membrane surface structure.

20 The delicate scrutiny of the surface structures shown in Fig. 2 reveals that the
21 membrane prepared by using ATBC had the spherulite with numerous small humps with a
22 diameter in nanoscale (50-300 nm). The magnified SEM images of Fig. 2(a-d) are shown in

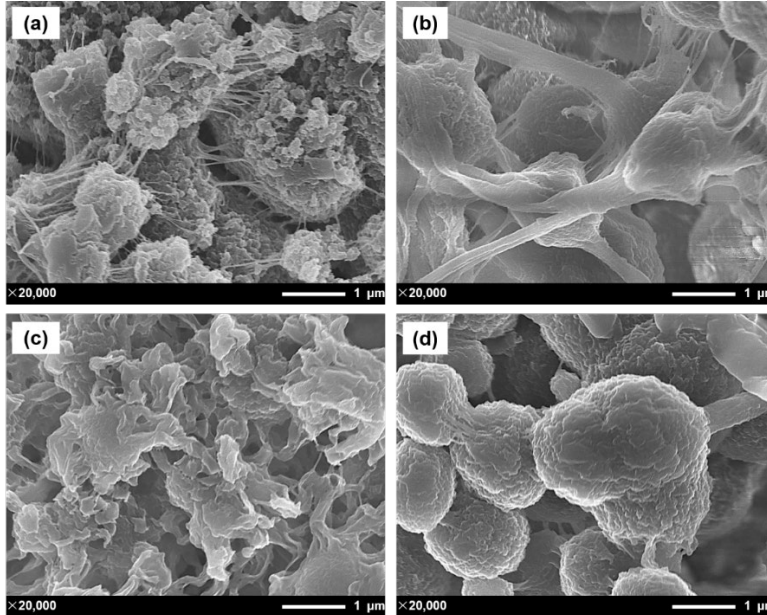
1 Fig. 4. Fig. 4(a) clearly shows the unique spherulite structure with the small humps when
2 co-extruding ATBC. Among four co-extruded solvents (ATBC, GTA, DEP, and PC), the
3 value of $|\delta_i(\text{ATBC})-\delta_i(\text{PVDF})|$ was the largest and much larger than that of PC, as shown in
4 Table 1 and Fig. 3. This suggests that the interaction between ATBC and PVDF is the
5 lowest and much lower than that between PC (diluent) and PVDF. Therefore, when ATBC
6 penetrates into the polymer solution during the co-extruding, the interaction between the
7 diluent (a mixture of PC and ATBC) and PVDF decreases. In the case of this interaction
8 decrease, the crystallization temperature increases, and thereby the nucleation rate increases
9 due to the large quenching depth, which induces the formation of smaller spherulites in a
10 nanoscale diameter [26]. Furthermore, the small spherulite forms just on the surface. The
11 humps on the spherulites are these small spherulites, and the aggregate of small and large
12 spherulites looks like the spherulite with many humps, as shown in Figs. 2(a) and 4(a), that
13 constructed a novel hierarchical spherulite structure.



1 **Fig. 2.** Outer surface SEM images of PVDF membrane prepared with and without co-
 2 extruded solvents. (a) ATBC; (b) GTA; (c) DEP; (d) PC; (e) Sulfolane; (f) GBL; (g) GC; (h)
 3 Normal PVDF membrane prepared without using co-extruded solvent.
 4



5
 6 **Fig. 3.** Ternary interaction among co-extruded solvents, PC (diluent), and PVDF (polymer).
 7



1

2 **Fig. 4.** Magnified outer surface SEM images of the prepared membranes with co-extruded
3 solvents. (a) ATBC; (b) GTA; (c) DEP; (d) PC.

4

5 **3.2. Membrane surface roughness and pore structure**

6 Figure 5 shows the membrane surface roughness in terms of different co-extruded
7 solvents. The normal PVDF membrane prepared without using co-extruded solvents showed
8 a relatively low surface roughness with an RMS value of about 1 μm . After extruding ATBC,
9 GTA, DEP, and PC at the membrane surface using the triple-orifice spinneret, the membrane
10 surface roughness increased with an RMS value of about 2 μm . However, other extruded
11 solvents used in this work, such as sulfolane, GBL, and GC, did not enhance the surface
12 roughness. The change in the membrane surface roughness agreed well with that of the
13 membrane surface morphology, as shown in Fig. 2. Hence, the increased membrane surface

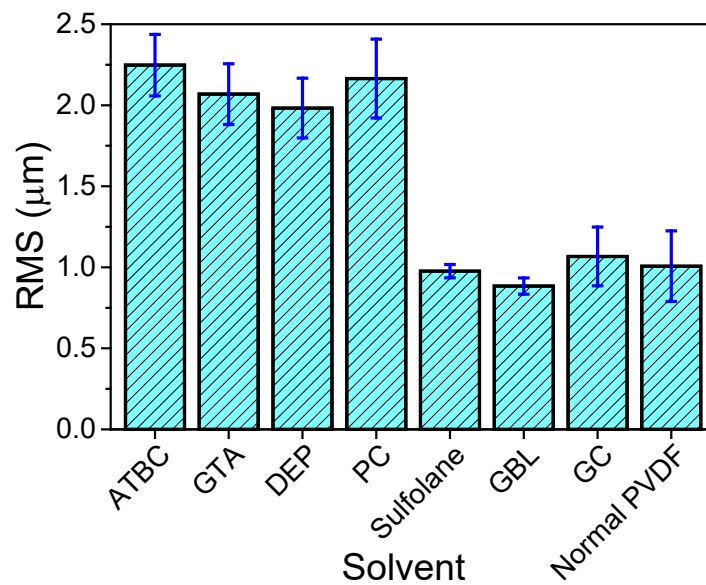
1 roughness can be explained by the isolated spherulite formation at the membrane surfaces in
2 the cases of ATBC, GTA, DEP, and PC extrusion (Fig. 2(a, b, c, and d)).

3 The effect of solvents on the membrane pore structure is shown in Table 2. The
4 surface porosity and pore size of the normal PVDF hollow fiber membrane prepared without
5 using co-extruded solvents could not be obtained using the software of ImageJ due to the
6 formed dense surface (Fig. 2(h)). When solvents, such as ATBC, GTA, DEP, and PC, were
7 extruded at the outer surface, the prepared membranes showed a surface porosity of about
8 20%, and the average surface pore size was about 400 nm with the maximum surface pore
9 size about 5000 nm. However, in the cases of sulfolane, GBL, and GC extrusion, due to the
10 formed dense surface structure similar to that of the normal PVDF membrane, the surface
11 porosity and pore size of the prepared membranes were not obtained.

12 Furthermore, the membrane mean pore size measured by a Liquid-Liquid porometer
13 are also shown in Table 2. The normal PVDF membrane and the PVDF membranes prepared
14 by co-extruding sulfolane, GBL, and GC had a small mean pore size of about 15-35 nm due
15 to the dense surface structure. However, by co-extruding ATBC, GTA, DEP, and PC, not
16 only the membrane surface pore size and porosity were enhanced as mentioned above, but
17 also the membrane mean pore size was increased to about 300 nm with 15 times higher than
18 that of the normal PVDF membrane (15 nm). The notably increased membrane pore size
19 greatly favors the water vapor permeation during the MD process.

20 In addition, the membrane bulk porosity was measured using the weight and volume
21 method (Table 2). All prepared membranes showed a similar bulk porosity about 70%, even
22 if the extruded solvents were used. This was because the bulk porosity mainly depends on

1 the diluent concentration in the polymer dope solution. In this work, the diluent was fixed at
 2 67 wt.% in all cases. These similar bulk porosities for all membranes are one of the evidences
 3 that the bulk structures were kept unchanged for all membranes.



4
 5 **Fig. 5.** Effect of co-extruded solvents on the membrane surface roughness.

6
 7 **Table 2.** Porosity and pore size of the prepared membranes.

	Surface porosity (%)	Average surface pore size (nm)	Maximum surface pore size (nm)	Mean pore size (nm)	Bulk porosity (%)
ATBC	19.3±0.5	368±12	4900±20	329±4	68.7±1.6
GTA	20.6±0.4	464±14	5000±40	331±2.4	67.4±1.8
DEP	21.6±0.7	459±8.0	5200±30	338±2.8	73.7±1.9
PC	22.8±0.2	475±21	5600±49	292±5.5	71.4±2.9
Sulfolane	*	*	*	37±1.7	68.3±1.5
GBL	*	*	*	17±1.3	70.8±3.2
GC	*	*	*	23±0.6	68.3±1.6
Normal PVDF	*	*	*	15±0.5	72.6±2.9

8 * Data could not be obtained due to the dense surface structure.

9
 10

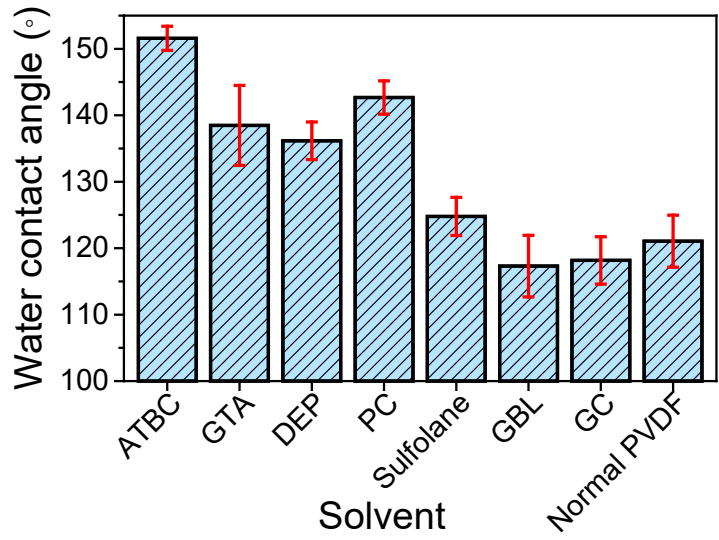
3.3. Membrane water contact angle and liquid entry pressure

Figure 6 shows the effect of co-extruding solvents on the PVDF membrane hydrophobicity. The WCA of the normal PVDF membrane was 121° and only slightly higher than the intrinsic WCA (108°) of PVDF with the smooth surface, due to the limiting surface roughness [8]. When co-extruding ATBC, GTA, DEP, and PC, the WCAs of the prepared PVDF membranes increased clearly to about 140° due to the increased surface roughness [27]. However, other extruded solvents including sulfolane, GBL, and GC did not enhance the membrane surface hydrophobicity because of their low ability in enhancing the membrane surface roughness (Fig. 5). Furthermore, although the membranes prepared using ATBC, GTA, DEP, and PC had a similar surface roughness with the RMS value of about $2\ \mu\text{m}$, as shown in Fig. 5, the membrane WCAs were different. The membrane prepared using ATBC showed the WCA of larger than 150° and achieved superhydrophobicity. This was further confirmed by the WCA hysteresis (Fig. 7). After attaching the water drop to the membrane surface, the water drop can be successfully pulled up from the membrane surface without any trails. By contrast, the membranes prepared by co-extruding the other three solvents, the WCAs were lower than 150° . For example, when using PC as the co-extruded solvent, the membrane WCA was 143° and the water drop could not be pulled up from the membrane surface, similar to the normal PVDF membrane prepared without extruding solvent (Fig. 7).

The co-extruding solvents showed a significant effect on the WCA. In addition to the surface roughness, this effect was mainly related to the tailored membrane surface structure. In this work, three surface structures were obtained by co-extruding solvents (Fig. 8). The

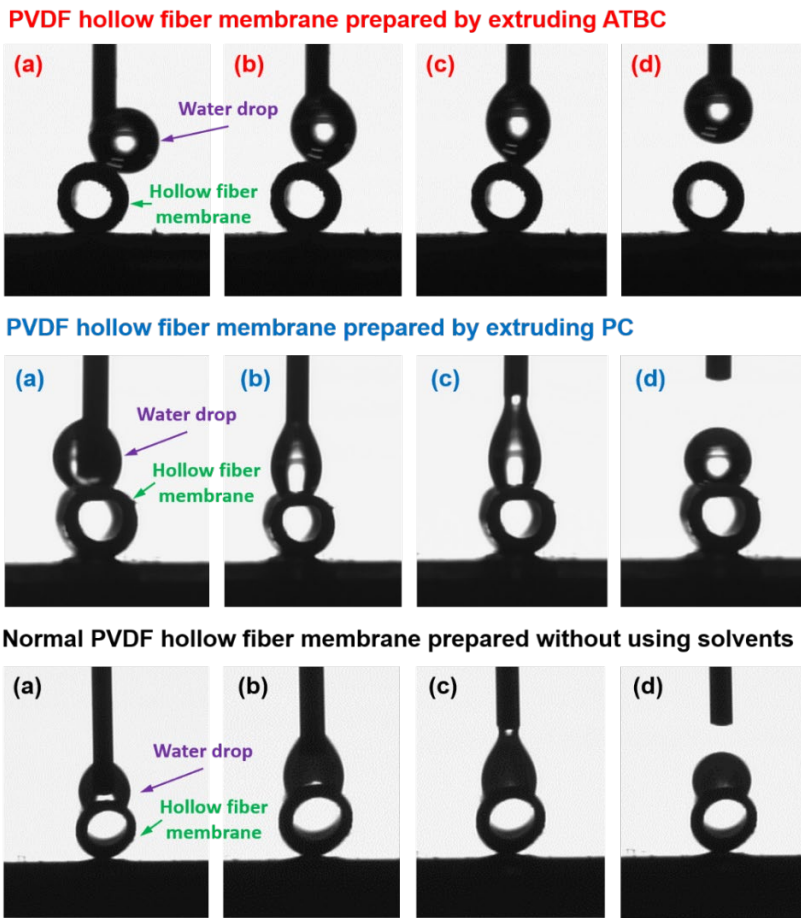
1 normal PVDF membrane and the PVDF membranes prepared by co-extruding sulfolane,
2 GBL, and GC had a dense and smooth surface (Fig. 2(e-f)) with contacted spherulites which
3 provided a low surface roughness (Fig. 5); so that the water drop can spread out that results
4 in a low WCA (Fig. 8(a)). When co-extruding ATBC, GTA, DEP, and PC, the prepared
5 membrane showed isolated spherulites on the surface (Figs. 2(a-d) and 4(a-d)). These isolated
6 spherulites decreased the contact area between the water drop and the membrane surface,
7 resulting in a high WCA, as shown in Fig. 8(b), because the air can be trapped in the space
8 between spherulites that can prevent the falling of water drop by gravity [28]. Among four
9 co-extruding solvents, ATBC induced the formation of many humps on the isolated
10 spherulite surface that constructed a novel hierarchical spherulite structure, as shown in Fig.
11 2(a) and 4(a). In the case, the water drop-membrane surface contact area could be further
12 decreased, which brought about the larger contact angle [29-31], as shown in Fig. 8(c), like
13 the nano-structures formed on the micro-structures of lotus surface [32-34]. Hence, the
14 membrane prepared by using ATBC showed a higher WCA compared to the membrane
15 prepared by GTA, DEP, and PC with only isolated spherulite surface structure and can
16 achieve superhydrophobicity.

17



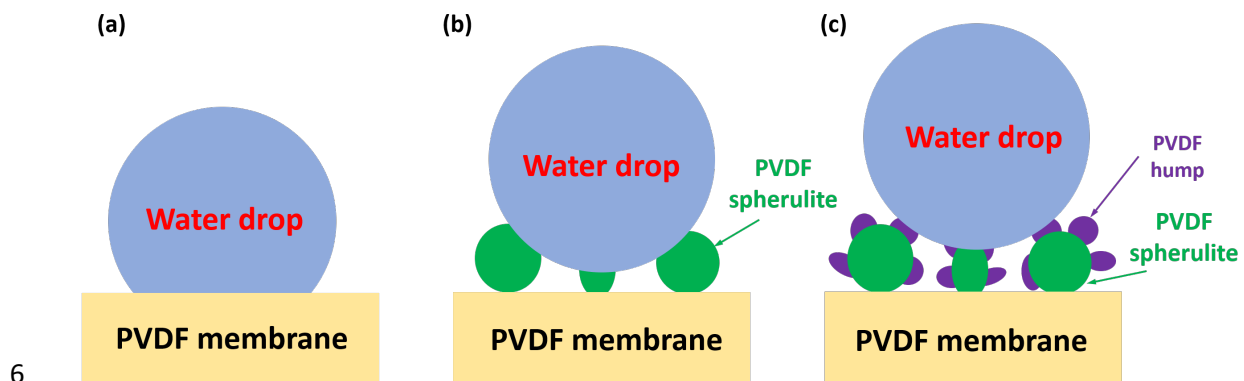
1

2 **Fig. 6.** Effect of co-extruded solvents on membrane water contact angle.



3

1 **Fig. 7.** Water contact angle hysteresis of the PVDF membranes prepared using ATBC (top)
2 and PC (middle), and the normal PVDF hollow fiber membrane prepared without using
3 solvents (bottom). (a) Water drop touching toward the membrane surface; (b) Pulling water
4 drop up slightly; (c) Pulling water drop up heavily; (d) Water drop departure from the
5 membrane surface.



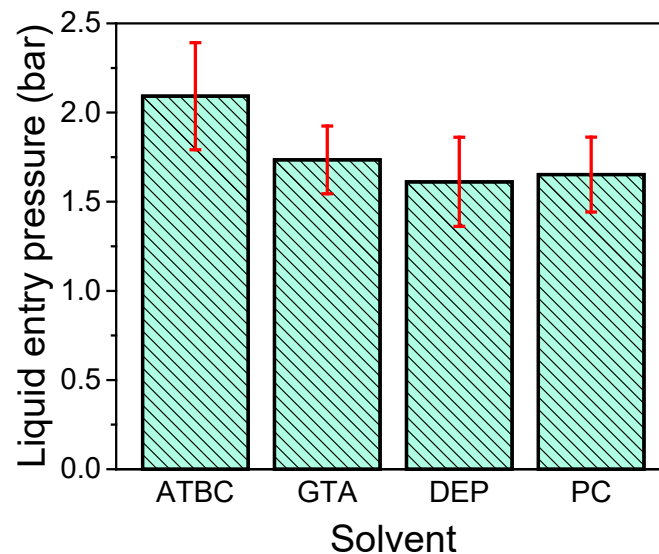
6
7 **Fig. 8.** Schematic of the effect of PVDF membrane surface spherulite morphology using this
8 new method with extruding solvents on the outermost layer on the membrane surface
9 hydrophobicity. (a) smooth surface. (b) spherulite surface without humps. (c) spherulite
10 surface with humps (hierarchical spherulite surface structure).

11
12 Liquid entry pressure (LEP) is a pressure that must be overcome for a liquid to pass
13 through a hydrophobic membrane. Thus, this is a significant parameter to evaluate the
14 membrane wetting resistance [35]. Usually, the LEP is affected by liquid surface tension,
15 membrane hydrophobicity, and membrane maximum pore size [35, 36]. In this work, the
16 membrane surface liquid entry pressure was investigated due to the formed spherulitic
17 structure and the tailored pore structure on the membrane surface and calculated based on the

1 water contact angle and the surface pore size. Figure 9 shows the membrane surface LEP
2 calculated using pure water as the media by the Cantor–Laplace equation (3) [36]:

$$3 \quad LEP = \frac{-2B\gamma\cos\theta}{r_{max}} \quad (3)$$

4 where B is a pore geometry coefficient and was set to 0.8 due to the irregularly shaped pores
5 of the prepared membranes in this work [35], γ is the water surface tension at 25 °C, 72 mN/m,
6 θ is the water contact angle, and r_{max} is the surface maximum pore size. The PVDF
7 membrane prepared by extruding ATBC showed the highest LEP due to the highest WCA
8 (Fig. 6) and the slightly lower surface maximum pore size (Table 2), compared to the
9 membranes prepared by extruding other three solvents. It could be anticipated that this high
10 LEP brings about the membrane with high wetting resistance during the MD operating.



11
12 **Fig. 9.** Surface liquid entry pressures of the PVDF membrane prepared using ATBC, GTA,
13 DEP, and PC.

1 **Can we include the results of mechanical strength here? One of the advantages using**
2 **the TIPs method is to improve it. As such, this would be important. You have the results**
3 **in Fig S5, which can be moved and discussed here.**

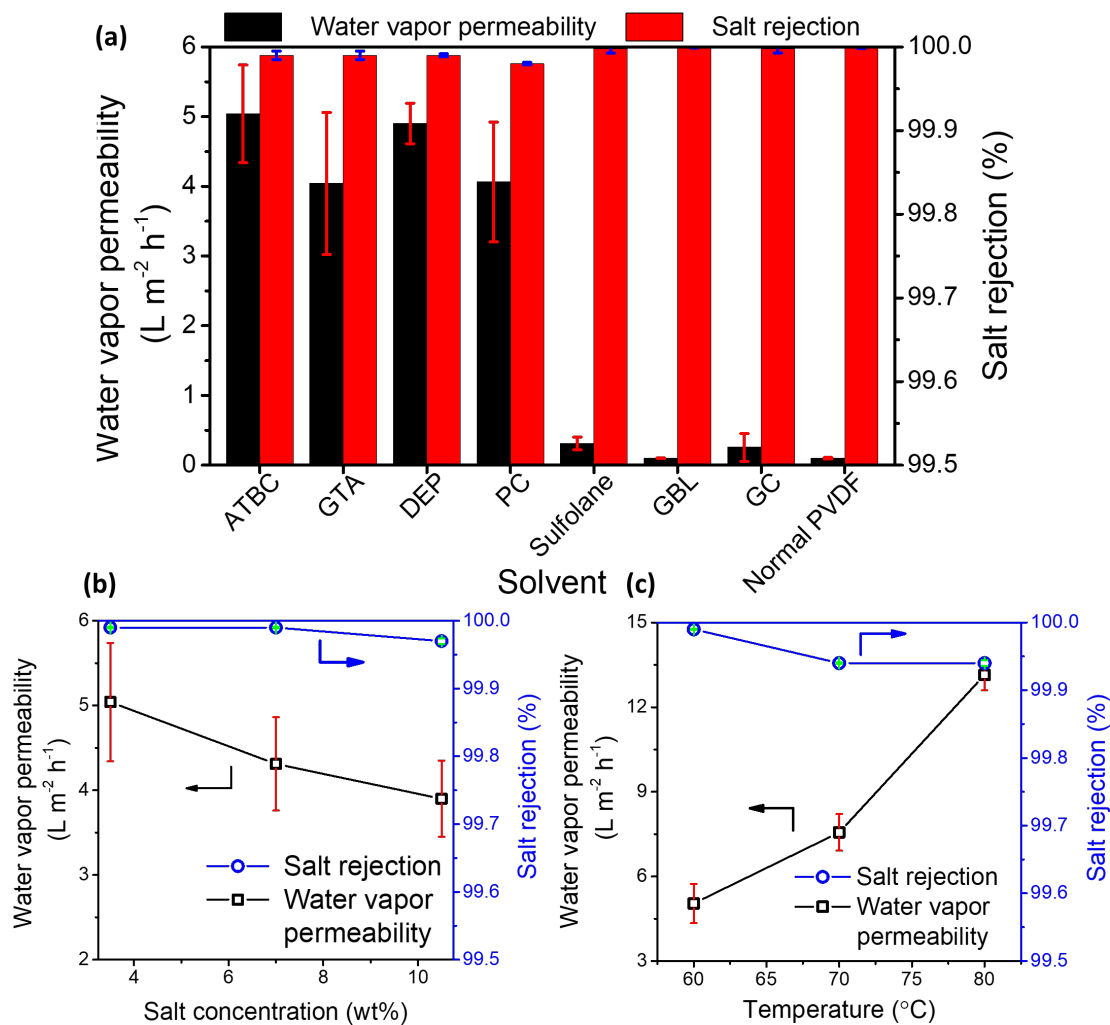
5 **3.4. Desalination performances by DCMD**

6 The desalination performances of the prepared membranes were evaluated using
7 DCMD (Fig. 10). In Fig. 10(a), the normal PVDF membrane prepared without extruding
8 solvents showed a quite low water vapor permeability about $0.1 \text{ L m}^{-2} \text{ h}^{-1}$. This is attributed
9 to its dense surface structure that impedes water vapor permeation. Furthermore, the low
10 water vapor permeabilities were also observed in the membranes prepared by extruding
11 sulfolane, GBL, and GC due to the dense surface structure similar to that of the normal PVDF
12 membrane. However, when extruding the other four solvents of ATBC, GTA, DEP, and PC,
13 the prepared membranes showed higher water vapor permeability about $5 \text{ L m}^{-2} \text{ h}^{-1}$ compared
14 to the normal PVDF membrane. On the other hand, all the prepared membranes showed
15 complete salt rejection . This was because all the prepared PVDF membranes were
16 hydrophobic with a WCA of more than 90° (Fig. 6), which successfully hindered the salt
17 water permeation through the membrane.

18 Furthermore, the effects of salt concentration and temperature of the feed solution on
19 the MD performance were evaluated using the PVDF membrane prepared by extruding
20 ATBC. In Fig. 10(b), with the increase of salt concentration, the water vapor permeability
21 decreased due to the decrease water vapor pressure caused by the decrease of water activity
22 [8, 37, 38]. On the other hand, due to the high hydrophobicity of the prepared membrane,

1 marginal effect on the salt rejection was observed, although increasing salt concentration
2 decreases the feed surface tension [6].

3 Figure 10(c) shows the effect of feed temperature on the MD performances. The
4 membrane water vapor permeability increased significantly to $13.5 \text{ L m}^{-2} \text{ h}^{-1}$ and was about
5 3 times higher than the initial one ($5.0 \text{ L m}^{-2} \text{ h}^{-1}$ at $60 \text{ }^\circ\text{C}$) at the temperature of $80 \text{ }^\circ\text{C}$. This
6 can be explained by the enhancing water vapor pressure and diffusion coefficient with
7 increasing temperature [8, 39]. According to the classic Antoine equation, it is known that
8 the vapor pressure enhances exponentially when increasing temperature [8], which
9 significantly favors the production of water vapor. On the other hand, only a slight decrease
10 in the salt rejection (0.04%) was observed with the increasing temperature, although
11 increasing temperature also decreases the feed surface tension [6].



1
2 **Fig. 10.** Membrane water vapor permeability and salt rejection. (a) Effect of solvent types.
3 Salt concentration: 35 g L^{-1} . Feed solution temperature: $60 \text{ }^{\circ}C$. (b) Effect of salt concentration.
4 Feed solution temperature: $60 \text{ }^{\circ}C$. The membrane prepared by extruding ATBC. (c) Effect of
5 feed solution temperature. Salt concentration: 35 g L^{-1} . The membrane prepared by extruding
6 ATBC.

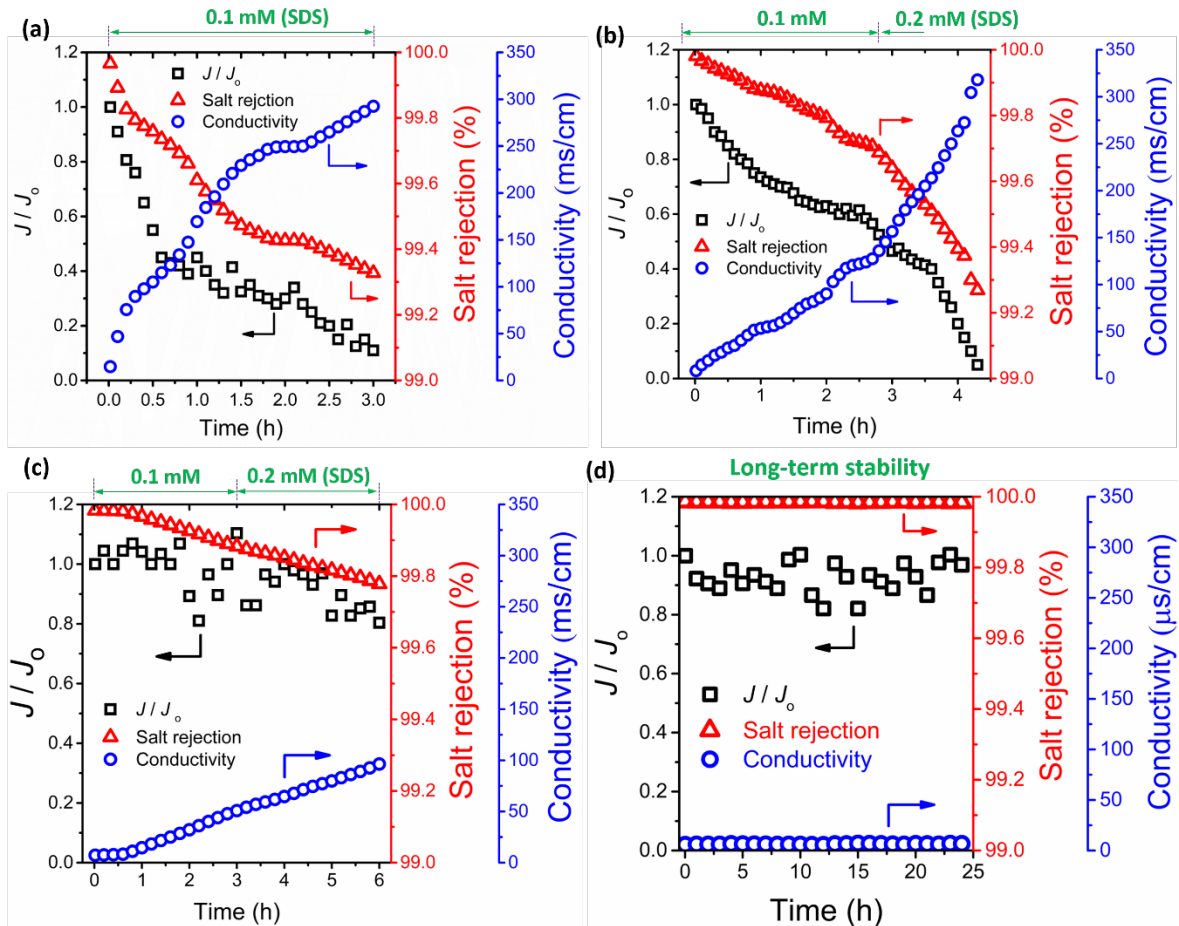
7
8 In addition to the permeability and rejection, the wetting resistance of the membrane
9 is of significant importance for maintaining high desalination performance by MD. However,

1 the membrane is usually wetted by the salt water solution in the real case because the real
2 seawater usually has some low-surface-tension organic compounds that are easy to wet the
3 membrane [40, 41], when the membrane hydrophobicity is insufficient. Once the membrane
4 is wetted, the membrane desalination performance decreases sharply, which is completely
5 unfavorable for the membrane application with high efficiency [6]. Here, a low-surface-
6 tension surfactant (SDS) with different concentrations was added into the salt water to assess
7 the membrane wetting resistance during the MD experiment. The results are shown in Fig.
8 11. Fig 11(a) shows the results of the normal PVDF membrane prepared without extruding
9 solvent. After adding 0.1 mM SDS, the surface tension decreased from 72 mN/m (no SDS)
10 to 48 mN/m (0.1 mM SDS) [9]. The water vapor permeability and salt rejection sharply
11 decreased due to the low wetting resistance of the normal membrane.

12 As shown in Fig. 11(b), after adding 0.1 mM SDS in the feed, the PVDF membrane
13 prepared by extruding PC showed higher retention in water vapor permeability (over 50%)
14 after 3 h, compared to that of the normal PVDF membrane (about 10 wt%) due to increased
15 hydrophobicity (Fig. 6). However, when the SDS concentration was enhanced to 0.2 mM,
16 the significant wetting occurred with a sharp decrease in water vapor permeability and salt
17 rejection, and remarkable increase in conductivity due to the further decrease in the surface
18 tension of the feed solution (41.4 mN/m of 0.2 mM SDS salt water) [9].

19 When the membrane prepared by extruding ATBC was used, even with the increase
20 of SDS concentration to 0.2 mM, the water vapor permeability of the membrane was still
21 more than 80% of the initial one with a high salt rejection of over 99.8%. In addition, as
22 shown in Fig. 11(d), the membrane showed long-term stability, in which the water vapor

1 permeability, salt rejection. and electrical conductivity of the permeated solution remained
 2 unchanged for 24 h, when the salt water without SDS was used as the feed solution. These
 3 high wetting resistances are attributed to the membrane superhydrophobicity (Figs. 6, 8, and
 4 9) caused by the special surface spherulite structure with lots of humps (Figs. 2(a) and 4(a)).



5
 6 **Fig. 11.** Membrane wetting resistance during MD experiment. (a) Normal PVDF membrane
 7 prepared using the PVDF concentration of 25 wt%. Feed solution: 35 g L⁻¹ salt water with
 8 0.1 mM SDS. The normal PVDF membrane used here was prepared by using the dope
 9 solution with a lower PVDF concentration of 25 wt% because the water vapor permeability
 10 of the normal PVDF membrane is quite low (Fig. 10(a)). The initial water vapor permeability

1 of this membrane was about $1.2 \text{ L m}^{-2} \text{ h}^{-1}$. (b) PVDF hollow fiber membrane prepared by
2 extruding PC. Feed solution: 35 g L^{-1} salt water with increasing SDS concentration. (c) PVDF
3 hollow fiber membrane prepared by extruding ATBC. Feed solution: 35 g L^{-1} salt water with
4 increasing SDS concentration. (d) Long-term stability of the PVDF membrane prepared by
5 extruding ATBC. Feed solution: 35 g L^{-1} salt water without SDS.

6
7 PVDF is well known to be a promising membrane material for the MD desalination.
8 However, due to its intrinsic hydrophobic limitation, the PVDF membrane is usually wetted
9 by the feed solution. Hence, great efforts have been made to enhance the PVDF membrane
10 hydrophobicity and wetting resistance. Some representative methods are listed in Table 3.
11 The new method developed in this work can provide the PVDF membrane with higher
12 wetting resistance than the common surface modification and blend methods using additional
13 materials including prefluoropholymers and nanoparticles. Although the wetting resistance
14 of our membrane was still lower than that of the PVDF membrane with omniphobicity by
15 double surface modification [42] or by double surface deposition of nanoparticles [10], our
16 method is much simpler due to the one-step procedure and no additional materials required.
17 This advantage of simplicity provides greater potential to scale-up for industrialization.

18

19

20

21 **Table 3.** Wetting resistance of the state-of-the-art PVDF membranes prepared using some
22 representative methods in MD operation.

Membrane	Method	Role	WCA / °	LEP / MPa	Permeability change with operating time	Permeability change with SDS solution	References
Sliver/PVDF nanocomposite	Surface loading silver nanoparticles	To increase surface roughness	153	0.15	6.7% decline after 6 h	*	[43]
Hyflon AD-decorated PVDF	Surface coating of hyflon AD amorphous perfluoropolymer	To reduce surface free energy	145	0.45	10% decline after 30 h	*	[11]
SiO ₂ /PVDF nanocomposite	Blending SiO ₂ nanoparticles	To increase surface roughness	139	0.38	2% decline after 6 h	*	[44]
CF ₄ -modified PVDF	CF ₄ plasma surface modification	To achieve omniphobicity	160	0.19	No change after 72 h	No change after 2 h (SDS: 0.5 mM)	[42]
Modified PVDF hollow fiber	Surface deposition of silica nanoparticles with subsequent Teflon AF 2400 coating	To achieve omniphobicity	148	*	*	10% decline after 2 h (SDS: 0.6 mM)	[10]
PDMS-PVDF	Electrospraying	To construct surface re-entrant structure	156	0.13	*	40% decline after 4 h (SDS: 0.2 mM)	[24]
PVDF hollow fiber	One step of co-extruding solvent in TIPS process to tailor spherulitic surface morphology	To construct surface micro-nano structure	151	0.2	No change after 24 h	20% decline after 3 h (SDS: 0.2 mM)	This work

* No data in references.

1
2

3 4. Conclusions

4 In this work, the novel PVDF hollow fiber membranes with unique spherulite surface
5 structures were prepared using a new method with co-extruding solvents at the outer layer of
6 the triple-orifice spinneret in the TIPS process. When ATBC, GTA, DEP, and PC were used
7 as the extruded solvents, the isolated spherulites were formed on the membrane surface,
8 which led to the higher surface roughness and the higher water contact angle. Especially, in
9 the case of ATBC, the hierarchical spherulite structure with lots of small humps was formed.
10 Owing to this special spherulite structure surface, the prepared membrane showed the
11 superhydrophobicity.

12 The prepared membranes were applied to MD process. The membrane prepared by
13 extruding ATBC showed high water vapor permeability ($13.5 \text{ L m}^{-2} \text{ h}^{-1}$), high salt rejection

1 of near 100%, and high wetting resistance for the low-surface-tension salt solution. This high
2 wetting resistance was attributed to the superhydrophobicity (water contact angle of larger
3 than 150°) caused by the novel hierarchical spherulite structure with humps.

4 Furthermore, the method developed in this work to confer the membrane with special
5 hierarchical spherulite surface structure and superhydrophobicity is a very simple one-step
6 process without additional materials. This simplicity is a great advantage for the preparation
7 of the hollow fiber membrane with high performances on a large scale.

8

9 **Conflicts of interest**

10 There are no conflicts to declare.

11

12 **Nomenclature**

13	A	outer surface area of the membrane (m^2)
14	$C_{F, \text{Salt}}$	NaCl concentration in feed solution (g L^{-1})
15	$C_{P, \text{Salt}}$	NaCl concentration in permeated solution (g L^{-1})
16	J	water vapor permeability ($\text{L m}^{-2} \text{h}^{-1}$)
17	m	permeated water mass (g),
18	t	permeation time (h)
19	V	permeation volume of pure water (L)
20	R_{salt}	salt rejection (%)
21	ρ	water density ($0.998\text{kg}\cdot\text{L}^{-1}$, 20°C)
22	LEP	liquid entry pressure (MPa)

1	δ_d	dispersion solubility parameter (MPa ^{0.5})
2	δ_p	polar solubility parameter (MPa ^{0.5})
3	δ_h	hydrogen bonding solubility parameter (MPa ^{0.5})
4	δ_t	total solubility parameter (MPa ^{0.5})
5	B	pore geometry coefficient
6	γ	water surface tension (mN/m)
7	θ	water contact angle (°)
8	r_{\max}	surface maximum pore size (nm)

9

10 **Acknowledgments**

11 Chuanjie Fang is grateful for the financial support from the China Scholarship Council (CSC,
 12 201808050053), China.

13

14

15 **References**

16

17

18

19 [1] M. Elimelech, W.A. Phillip, The future of seawater desalination: energy, technology, and the
 20 environment, *Science*, 333 (2011) 712-717.

21 [2] M. Khayet, Membranes and theoretical modeling of membrane distillation: a review, *Adv. Colloid
 22 Interface Sci.*, 164 (2011) 56-88.

23 [3] S. Lin, S. Nejati, C. Boo, Y. Hu, C.O. Osuji, M. Elimelech, Omniphobic Membrane for Robust
 24 Membrane Distillation, *Environ. Sci. Technol. Lett.*, 1 (2014) 443-447.

25 [4] L.D. Tijing, Y.C. Woo, J.-S. Choi, S. Lee, S.-H. Kim, H.K. Shon, Fouling and its control in
 26 membrane distillation—A review, *J. Membr. Sci.*, 475 (2015) 215-244.

- 1 [5] M. Pagliero, A. Bottino, A. Comite, C. Costa, Novel hydrophobic PVDF membranes prepared by
2 nonsolvent induced phase separation for membrane distillation, *J. Membr. Sci.*, 596 (2020) 117575.
- 3 [6] M. Rezaei, D.M. Warsinger, V.J. Lienhard, M.C. Duke, T. Matsuura, W.M. Samhaber, Wetting
4 phenomena in membrane distillation: Mechanisms, reversal, and prevention, *Water Res.*, 139 (2018)
5 329-352.
- 6 [7] E. Guillen-Burrieza, M.O. Mavukkandy, M.R. Bilad, H.A. Arafat, Understanding wetting
7 phenomena in membrane distillation and how operational parameters can affect it, *J. Membr. Sci.*,
8 515 (2016) 163-174.
- 9 [8] A. Alkhudhiri, N. Darwish, N. Hilal, Membrane distillation: A comprehensive review,
10 *Desalination*, 287 (2012) 2-18.
- 11 [9] C. Boo, J. Lee, M. Elimelech, Engineering Surface Energy and Nanostructure of Microporous
12 Films for Expanded Membrane Distillation Applications, *Environ. Sci. Technol.*, 50 (2016) 8112-
13 8119.
- 14 [10] K.J. Lu, J. Zuo, J. Chang, H.N. Kuan, T.S. Chung, Omniphobic Hollow-Fiber Membranes for
15 Vacuum Membrane Distillation, *Environ. Sci. Technol.*, 52 (2018) 4472-4480.
- 16 [11] Y. Zhang, X. Wang, Z. Cui, E. Drioli, Z. Wang, S. Zhao, Enhancing wetting resistance of
17 poly(vinylidene fluoride) membranes for vacuum membrane distillation, *Desalination*, 415 (2017)
18 58-66.
- 19 [12] D. Zhao, J. Zuo, K.-J. Lu, T.-S. Chung, Fluorographite modified PVDF membranes for seawater
20 desalination via direct contact membrane distillation, *Desalination*, 413 (2017) 119-126.
- 21 [13] C. Fang, S. Jeon, S. Rajabzadeh, L. Fang, L. Cheng, H. Matsuyama, Tailoring the surface pore
22 size of hollow fiber membranes in the TIPS process, *J. Mater. Chem. A*, 6 (2018) 535-547.
- 23 [14] C. Fang, S. Jeon, S. Rajabzadeh, L. Fang, L. Cheng, H. Matsuyama, Tailoring both the surface
24 pore size and sub-layer structures of PVDF membranes prepared by the TIPS process with a triple
25 orifice spinneret, *J. Mater. Chem. A*, 6 (2018) 20712-20724.
- 26 [15] C. Fang, S. Rajabzadeh, W. Liu, H.-C. Wu, N. Kato, Y. Sun, S. Jeon, H. Matsuyama, Effect of
27 mixed diluents during thermally induced phase separation process on structures and performances of
28 hollow fiber membranes prepared using triple-orifice spinneret, *J. Membr. Sci.*, 596 (2020) 117715.
- 29 [16] C. Fang, S. Rajabzadeh, H.-C. Wu, X. Zhang, N. Kato, M. Kunitatsu, T. Yoshioka, H.
30 Matsuyama, Effect of mass transfer at the interface of the polymer solution and extruded solvent
31 during the air gap on membrane structures and performances in TIPS process using triple-orifice
32 spinneret, *J. Membr. Sci.*, 595 (2020) 117513.

- 1 [17] I.J. Roh, S. Ramaswamy, W.B. Krantz, A.R. Greenberg, Poly(ethylene chlorotrifluoroethylene)
2 membrane formation via thermally induced phase separation (TIPS), *J. Membr. Sci.*, 362 (2010) 211-
3 220.
- 4 [18] J.T. Jung, H.H. Wang, J.F. Kim, J. Lee, J.S. Kim, E. Drioli, Y.M. Lee, Tailoring nonsolvent-
5 thermally induced phase separation (N-TIPS) effect using triple spinneret to fabricate high
6 performance PVDF hollow fiber membranes, *J. Membr. Sci.*, 559 (2018) 117-126.
- 7 [19] S. Bonyadi, T.-S. Chung, Highly porous and macrovoid-free PVDF hollow fiber membranes for
8 membrane distillation by a solvent-dope solution co-extrusion approach, *J. Membr. Sci.*, 331 (2009)
9 66-74.
- 10 [20] C. Fang, S. Rajabzadeh, P. Zhang, W. Liu, N. Kato, H.K. Shon, H. Matsuyama, Controlling
11 spherulitic structures at surface and sub-layer of hollow fiber membranes prepared using nucleation
12 agents via triple-orifice spinneret in TIPS process, *J. Membr. Sci.*, (2020) 118229.
- 13 [21] C.M. Hansen, Hansen solubility parameters: a user's handbook, CRC press, 2007.
- 14 [22] N.L. Cheng, Solvents Handbook, Chinese Chemical Industry Press, Beijing China, 2002.
- 15 [23] C. Fang, S. Rajabzadeh, H.-C. Wu, X. Zhang, N. Kato, M. Kunitatsu, T. Yoshioka, H.
16 Matsuyama, Effect of mass transfer at the interface of the polymer solution and extruded solvent
17 during the air gap on membrane structures and performances in TIPS process using triple-orifice
18 spinneret, *J. Membr. Sci.*, (2019) 117513.
- 19 [24] E.J. Lee, B.J. Deka, J. Guo, Y.C. Woo, H.K. Shon, A.K. An, Engineering the Re-Entrant
20 Hierarchy and Surface Energy of PDMS-PVDF Membrane for Membrane Distillation Using a Facile
21 and Benign Microsphere Coating, *Environ. Sci. Technol.*, 51 (2017) 10117-10126.
- 22 [25] D.R. Lloyd, S.S. Kim, K.E. Kinzer, Microporous membrane formation via thermally-induced
23 phase separation. II. Liquid-liquid phase separation, *J. Membr. Sci.*, 64 (1991) 1-11.
- 24 [26] D.R. Lloyd, K.E. Kinzer, H.S. Tseng, Microporous membrane formation via thermally induced
25 phase separation. I. Solid-liquid phase separation, *J. Membr. Sci.*, 52 (1990) 239-261.
- 26 [27] R.N. Wenzel, Resistance of Solid Surfaces to Wetting by Water *Ind. Eng. Chem.* , 28 (1936)
27 988-994.
- 28 [28] A. Cassie, S. Baxter, Wettability of porous surfaces, *Transactions of the Faraday society*, 40
29 (1944) 546-551.
- 30 [29] M. Nosonovsky, Multiscale Roughness and Stability of Superhydrophobic Biomimetic
31 Interfaces, *Langmuir*, 23 (2007) 3157-3161.

- 1 [30] A. Tuteja, W. Choi, M. Ma, J.M. Mabry, S.A. Mazzella, G.C. Rutledge, G.H. McKinley, R.E.
2 Cohen, Designing Superoleophobic Surfaces, *Science*, 318 (2007) 1618.
- 3 [31] A. Tuteja, W. Choi, J.M. Mabry, G.H. McKinley, R.E. Cohen, Robust omniphobic surfaces,
4 *Proceedings of the National Academy of Sciences*, 105 (2008) 18200.
- 5 [32] L. Feng, S. Li, Y. Li, H. Li, L. Zhang, J. Zhai, Y. Song, B. Liu, L. Jiang, D. Zhu, Super -
6 hydrophobic surfaces: from natural to artificial, *Adv. Mater.*, 14 (2002) 1857-1860.
- 7 [33] X.J. Feng, L. Jiang, Design and Creation of Superwetting/Antiwetting Surfaces, *Adv. Mater.*, 18
8 (2006) 3063-3078.
- 9 [34] D. Ebert, B. Bhushan, Durable Lotus-effect surfaces with hierarchical structure using micro- and
10 nanosized hydrophobic silica particles, *J Colloid Interface Sci*, 368 (2012) 584-591.
- 11 [35] Z. Wang, Y. Chen, X. Sun, R. Duddu, S. Lin, Mechanism of pore wetting in membrane
12 distillation with alcohol vs. surfactant, *J. Membr. Sci.*, 559 (2018) 183-195.
- 13 [36] A.C.M. Franken, J.A.M. Nolten, M.H.V. Mulder, D. Bargeman, C.A. Smolders, Wetting criteria
14 for the applicability of membrane distillation, *J. Membr. Sci.*, 33 (1987) 315-328.
- 15 [37] K.W. Lawson, D.R. Lloyd, Membrane distillation, *J. Membr. Sci.*, 124 (1997) 1-25.
- 16 [38] M. Qtaishat, T. Matsuura, B. Kruczek, M. Khayet, Heat and mass transfer analysis in direct
17 contact membrane distillation, *Desalination*, 219 (2008) 272-292.
- 18 [39] A.M. Alklaibi, N. Lior, Membrane-distillation desalination: Status and potential, *Desalination*,
19 171 (2005) 111-131.
- 20 [40] Y.X. Huang, Z. Wang, J. Jin, S. Lin, Novel Janus Membrane for Membrane Distillation with
21 Simultaneous Fouling and Wetting Resistance, *Environ. Sci. Technol.*, 51 (2017) 13304-13310.
- 22 [41] M. Rezaei, D.M. Warsinger, J.H. Lienhard V, W.M. Samhaber, Wetting prevention in membrane
23 distillation through superhydrophobicity and recharging an air layer on the membrane surface, *J.*
24 *Membr. Sci.*, 530 (2017) 42-52.
- 25 [42] Y. Chul Woo, Y. Chen, L.D. Tijing, S. Phuntsho, T. He, J.-S. Choi, S.-H. Kim, H. Kyong Shon,
26 CF₄ plasma-modified omniphobic electrospun nanofiber membrane for produced water brine
27 treatment by membrane distillation, *J. Membr. Sci.*, 529 (2017) 234-242.
- 28 [43] Y. Liao, R. Wang, A.G. Fane, Engineering superhydrophobic surface on poly(vinylidene fluoride)
29 nanofiber membranes for direct contact membrane distillation, *J. Membr. Sci.*, 440 (2013) 77-87.

- 1 [44] J.E. Efome, D. Rana, T. Matsuura, C.Q. Lan, Enhanced performance of PVDF nanocomposite
- 2 membrane by nanofiber coating: A membrane for sustainable desalination through MD, *Water Res.*,
- 3 89 (2016) 39-49.
- 4

Supporting information

Hollow fiber membranes with hierarchical spherulite surface structure prepared by TIPS process using triple-orifice spinneret for high-efficiency membrane distillation

Chuanjie Fang ^a, Wenyi Liu ^a, Pengfei Zhang ^a, Saeid Rajabzadeh ^a, Noriaki Kato ^a, Yuji Sasaki ^a, Ho Kyong Shon ^b, Hideto Matsuyama ^{a*}

^a *Research Center for Membrane and Film Technology, Department of Chemical Science and Engineering, Kobe University, Rokkodaicho 1-1, Nada, Kobe 657-8501, Japan*

^b *Centre for Technology in Water and Wastewater (CTWW), School of Civil and Environmental Engineering, University of Technology, Sydney (UTS), P.O. Box 123, Broadway, NSW 2007, Australia*

** Corresponding author: Professor H. Matsuyama*

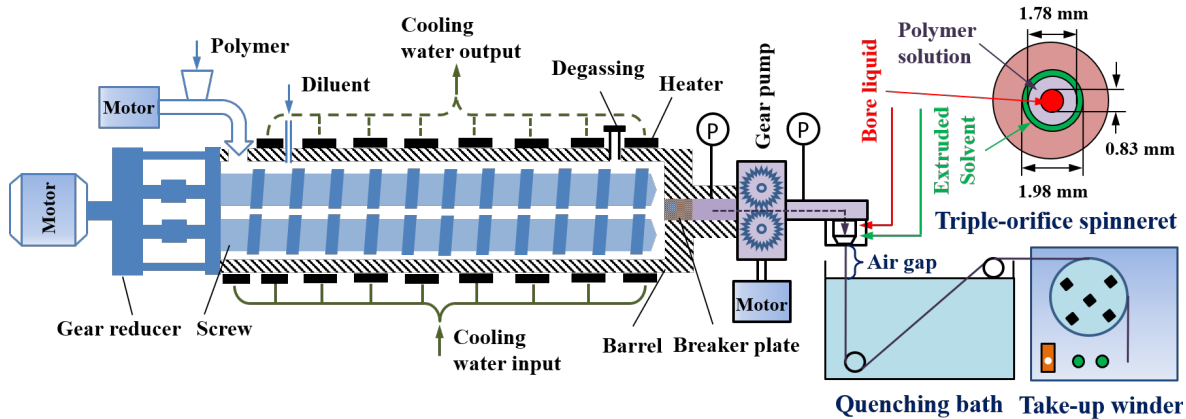
E-mail address: matuyama@kobe-u.ac.jp (H. Matsuyama)

Tel. / Fax: +81 78 803 6180

1 **1. Membrane preparation**

2 A schematic of the membrane preparation apparatus using a two-screw extruder
3 (TW05, ULTnano, Japan) and triple-orifice spinneret (Kasen Nozzle Mfg. Co., Ltd., Japan)
4 is shown in Fig. S1. Propylene carbonate (PC) used as a diluent flowed into the extruder at
5 190 °C at a flow rate of 6.12 g min⁻¹ controlled by a gear pump (5GU30KB, Oriental Motor
6 Co., Ltd., Japan). PVDF was fed into the extruder at a constant rate of 2.38 g min⁻¹. The rates
7 of PC and PVDF were determined based on the fixed concentrations (PVDF: 33 wt%, PC:
8 67wt%). After releasing the air bubbles in the heated zones of the extruder barrel, the
9 homogenous polymer solution was transported to a gear pump (Kawasaki Heavy Industry
10 LTD, Japan) at a pressure of 1.5 MPa. The gear pump forced the PVDF solution through the
11 middle channel of the triple-orifice spinneret at a constant rate of 8.5 g min⁻¹. The details of
12 the triple-orifice spinneret are also shown in Fig. S1. In the inner channel of the spinneret,
13 PC used as a bore liquid was extruded via a gear pump (5GU30KB, Oriental Motor Co., Ltd.,
14 Japan) to form the lumen of hollow fibers. Solvent (Table 1) simultaneously flowed through
15 the outermost channel of the triple orifice spinneret at a constant rate of 2 g min⁻¹, driven by
16 a peristaltic pump (Chuo Rika LTD, Japan). The solvent was used to tailor the surface
17 structure of PVDF hollow fiber membranes. After passing through an air gap distance of 10
18 cm, the extruded hollow fibers were immersed in a water quenching bath (5 °C) to induce
19 phase separation and solidification and then wound on a take-up winder. The diluent (PC) in
20 the prepared membrane was extracted via immersion in ethanol at room temperature for at
21 least 1 week and then the membrane was moved into pure water for two days to replace the
22 ethanol. Finally, the prepared membranes were dried at room temperature and then stored for
23 subsequent characterization and tests. Table S1 shows the conditions and parameters of the
24 hollow fiber membrane preparation. A normal PVDF membrane was prepared with the same
25 conditions while without extruding solvent for the comparison of using extruded solvents.

26 In addition, another normal PVDF hollow fiber membrane with a lower PVDF
27 concentration of 25 wt% was prepared to investigate the effect of PVDF concentration on the
28 water vapor permeability when extruding solvents was not used.



1
2
3
4
5

6
7
8
9
10
11

Fig. S1. Two-screw extruder and triple-orifice spinneret for the preparation of hollow fiber membranes in the TIPS process.

Table S1 PVDF hollow fiber membrane preparation conditions.

Preparation condition	Parameter
PVDF concentration (wt.%)	33
Diluent concentration (wt.%)	67
Screw temperature (°C)	190
Screw speed (rpm)	100
PVDF solution extruded rate (g min ⁻¹)	8.5
Bore liquid	PC
Bore liquid flow rate (mL min ⁻¹)	5.5
Extruded material	Solvent
Extruded NA solution flow rate (mL min ⁻¹)	2
Air gap (cm)	10
Water quenching bath temperature (°C)	5
Take-up speed (m min ⁻¹)	20

1 **Table S2** Diameters and thickness of PVDF hollow fiber membranes.

	Outer diameter (mm)	Inner diameter (mm)	Thickness (mm)
ATBC	1.1	0.69	0.22
GTA	1.2	0.77	0.20
DEP	1.1	0.71	0.20
PC	1.1	0.63	0.23
Sulfolane	1.2	0.71	0.23
GBL	1.1	0.67	0.22
GC	1.1	0.61	0.22
PVDF	1.3	0.73	0.26

2

3 **2. Membrane bulk porosity test**

4 Membrane bulk porosity was determined by measuring weight and volume [1]. Wet
 5 membrane was collected from water bath and cut to 5 cm in length (l), and subsequently
 6 freeze-dried overnight before the weight (m) of giving samples was balanced. Membrane
 7 bulk porosity, ε (%), was computed using equation S1:

$$8 \quad \varepsilon = \frac{\frac{1}{4}\pi l \rho (OD^2 - ID^2) - m}{\frac{1}{4}\pi l \rho (OD^2 - ID^2)} \times 100 \quad (S1)$$

9 where OD and ID are the membrane outer and inner diameters (mm), respectively, and ρ is
 10 the PVDF density (g/cm).

11

12

13

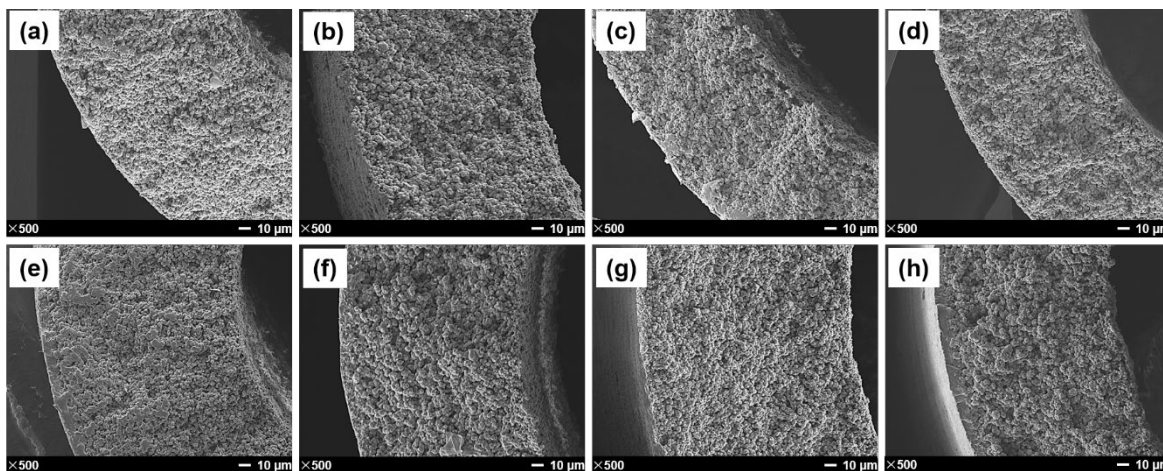
14

15

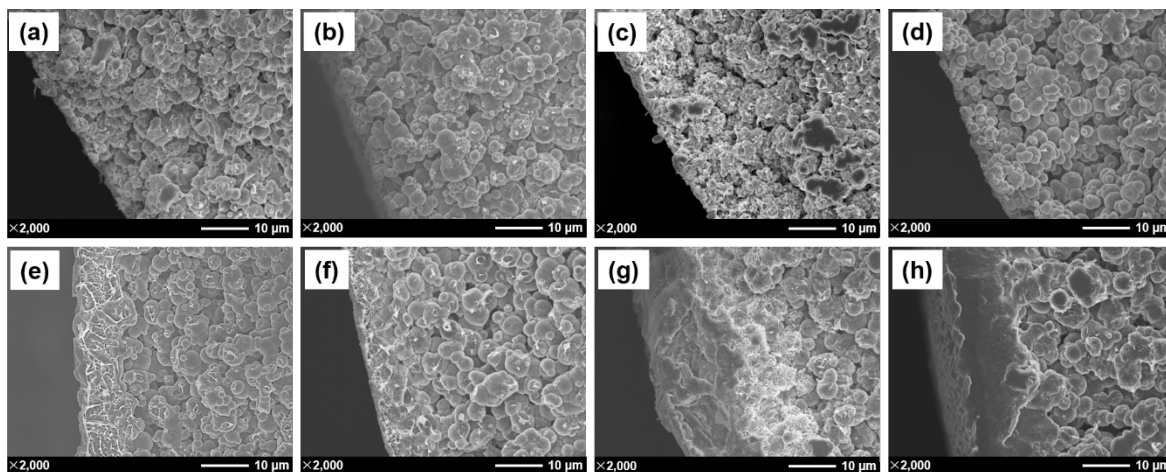
16

17

1 **3. Membrane morphology**

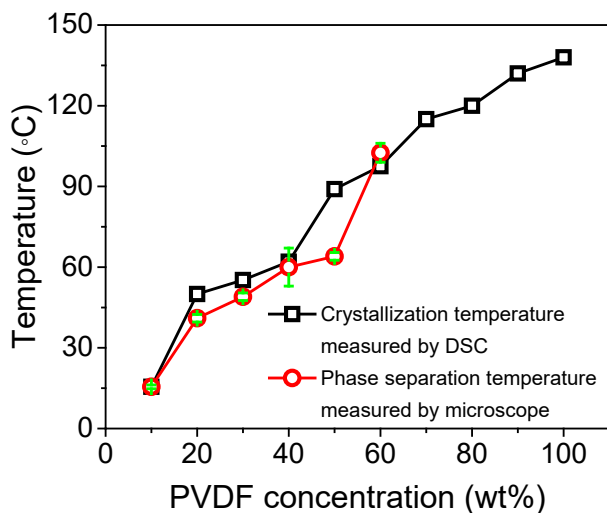


7 **Fig. S2.** SEM images of cross-section of PVDF membranes prepared with and without using
8 solvents. (a) ATBC; (b) GTA; (c) DEP; (d) PC; (e) Sulfolane; (f) GBL; (g) GC; (h) Normal
9 PVDF membrane prepared without using solvents.
10



7 **Fig. S3.** SEM images of cross-section near the outer surface of PVDF membranes prepared
8 with and without using solvents. (a) ATBC; (b) GTA; (c) DEP; (d) PC; (e) Sulfolane; (f)
9 GBL; (g) GC; (h) Normal PVDF membrane prepared without using solvents.
10

1 **4. Phase diagram**



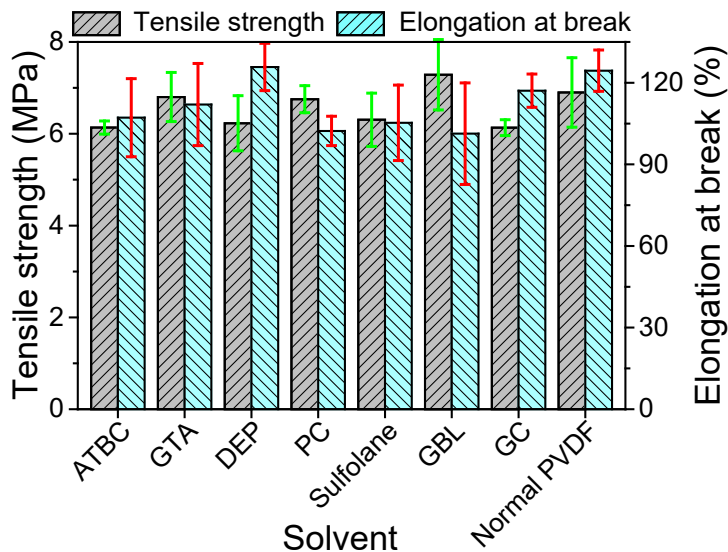
2

3 **Fig. S4.** Phase diagram of PVDF solution prepared using PC as the diluent [2].

4 Fig. S4 shows the phase diagram of the PVDF/PC system. The phase separation
 5 temperatures observed by the microscope agreed with the crystallization temperatures
 6 measured by DSC. This indicates the phase separation mechanism of the system during
 7 cooling was the typical solid-liquid (S-L) phase separation.

8

9 **5. Mechanical strength**



10

11 **Fig. S5.** Effect of solvents on the mechanical strength of PVDF hollow fiber membranes.

1 **References**

2 [1] C. Fang, S. Jeon, S. Rajabzadeh, L. Fang, L. Cheng, H. Matsuyama, Tailoring the surface pore
3 size of hollow fiber membranes in the TIPS process, *J. Mater. Chem. A*, 6 (2018) 535-547.

4 [2] C. Fang, S. Rajabzadeh, H.-C. Wu, X. Zhang, N. Kato, M. Kunimatsu, T. Yoshioka, H.
5 Matsuyama, Effect of mass transfer at the interface of the polymer solution and extruded solvent
6 during the air gap on membrane structures and performances in TIPS process using triple-orifice
7 spinneret, *J. Membr. Sci.*, 595 (2020) 117513.

8

9